

INNOVATIVE DIAGNOSTICS FOR THERMAL PLASMA PROCESSES

E. SIEWERT, B. BACHMANN, M. KÜHN-KAUFFELDT AND J. SCHEIN*

Universität der Bundeswehr München, Lab. f. Plasma Technology, 85577, Neubiberg, Germany
*js@unibw.de

ABSTRACT

The diagnostic of thermal plasmas is the main source of knowledge about technological applications like welding, cutting or thermal spray and is an enabling technology for the development and use of numerical simulation. Numerous analytical systems have been developed and applied to determine parameters like particle density, temperature or electrode behaviour. With the advent of new challenges especially due to advances in materials science innovative diagnostic systems are needed to determine phenomena like transient plasma behaviour or electrode phenomena especially in non-rotationally symmetric systems or during interaction with materials immersed inside the plasma. Fast system are introduced in this paper enabling the determination of temperatures, densities or plasma-conductor interaction involving the use of high-speed cameras employing spectrally resolved imaging to provide temporally resolved information about transient plasma processes.

1. INTRODUCTION

Thermal plasmas have been the subject of detailed experimental investigations for over 100 years. Applications like welding, cutting, thermal spray or -more recently- waste destruction are used in numerous variations which have an enormous impact on quality and cost of a wide range of commercial products. In this paper we will focus on two applications and their performance evaluation: welding and thermal spray.

The pulsed gas metal arc welding (PGMAW) process is widely used due to its universal applicability, high deposition rate and automatic feeding of the filler material and has therefore an immense industrial relevance. However there is still a great need for developments, such as e.g. reduction of emissions [1-4] and spatter, increase of process stability, expansion of process limits

or reduction of heat input into the workpiece. Finally it is desired to predict resulting weld seam properties as a function of process settings without time-consuming test series. Therefore a better understanding of the complex physical and chemical transactions is required [4]. In particular transient temperature evaluation, droplet formation, droplet detachment and interaction of material transfer with the weld seam formation is up to now poorly understood [5]. Unfortunately the material transfer is difficult to analyze experimentally due to a high droplet detachment frequency, high plasma temperature and intense plasma radiation. Simulation [2, 6-11] may provide new possibilities to improve process understanding and process development, but important thermophysical parameters are still missing to develop and validate accurate models. Such parameters are temperature of the plasma and temperature, viscosity and surface tension of wire tip and droplet. Diagnostic techniques to determine these properties are described in detail in [12] and summarized in this paper.

Thermal spray is one of the most potent tools for producing thick coatings. The principle of operation is based on a heat source, which under the influence of a strong gas flow, results in a high velocity hot stream of gas. Particles are inserted into the jet, which are heated and accelerated towards a substrate where they arrive as splats to build up upon each other to form a coating. Various technologies are currently in use which can be distinguished by the heat source [13].

A fairly common system is the so called plasma spray technology [14], which, when used at atmospheric pressure, will heat up particles in various sizes ranging from metals to ceramics by passing it through a plasma jet of about 15000 K at the nozzle exit [15], accelerating these particles to a speed of up to 300 m/s.

Even though plasma spray is an established technology there are still issues that, when solved, could lead to significant improvements of the process. For once the entrainment of the particles into the plasma jet which are usually carried by a cold gas flow is still an issue. [16]. Another major problem is based on the design of the plasma torches where the position of the anode attachment can and will change, mostly due to the strong gas flow. This is partly intentional and also enhanced by a vortex component to the axial gas flow as short residence times of the anodic arc root prevent local overheating and melting of the anode surface [17], but it also leads to variations in arc length, and thus to arc voltage/power fluctuations [18], [19]. These fluctuations are also reflected by variations in plasma jet length as high speed images reveal [20], which are shown in Figure 3 where the change in jet length and luminosity in a frequency range of ~ 50 kHz is nicely depicted [21].

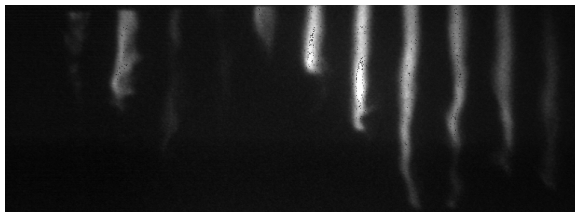


Figure 1: Fluctuations of a jet generated by a F4 torch, each jet recorded every 20 μ s, exposure time 5 ns, 6 mm nozzle diameter, plasma gas 45/12 slpm Ar/N₂, current 540 A

As the plasma jets are responsible for particle heating their structure is still a subject of ongoing research and will be discussed in this paper.

2. WELDING APPLICATIONS

Due to the increase of highly dynamic plasma processes the determination of transient plasma temperatures and related parameters like densities of atomic species or electrical conductivity gains importance in the field of plasma processing. Here we present a technique that accomplishes these goals and meets the demand for a non-intrusive, high-speed and three-dimensional plasma diagnostic, which is the adaption of the spectroscopic 'two line' method using high-speed camera imaging.

This method has been validated using different spectroscopic techniques to compare the results during a stationary process [22]. For simplicity we restrict ourselves to the tungsten inert gas (TIG) welding process with pure Argon as shielding gas. Our approach is as follows: Plasma temperature is derived by the comparison

of the detected plasma radiation with a calculated plasma emission assuming an optically thin plasma gas and a single local temperature for all plasma gas species. The spectral emission coefficient is calculated for the spectral bands defined by the used filter characteristics, based on the emission of lines and continuum. Plasma radiation is subsequently measured by means of a high-speed camera for the two short spectral bands simultaneously at high speed and spatially reconstructed by an Abel inversion procedure. The ratio of local emission coefficients from the two spectral intervals measured with the filter based setup is compared to the calculated emission spectra and thereby correlated with temperature.

The experimental setup is shown in Figure 2.

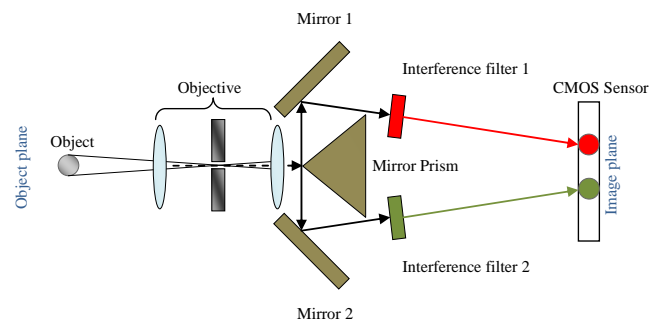


Figure 2, the object of interest is observed through an objective. The collected light is divided into two beams by a mirror prism. Both beams are projected onto a low light performance CMOS image sensor of a high speed camera (pco dimax) by two mirrors. In both beam paths an interference filter of different wavelengths is placed, thus two images of the same object in different wavelength interval are obtained

A setup of mirrors allows for synchronous imaging of the arc at two different wavelength intervals on a single camera chip. This enables high-speed three-dimensional determination (in case of axial symmetry) of plasma parameters like temperature and densities of atomic species. The wavelength intervals, which are defined by the spectral interference filter in each optical path. A typical image resulting from such a setup is shown in Figure 3 for 487.5 to 488.5 nm (left) and 689 to 699 nm (right). Each center wavelength of a filter was selected according to measurements showing that plasma is optically thin in the employed spectral bands. The {full width at half maximum} (1nm FWHM and 10nm FWHM, respectively) of each filter was selected to yield a similar radiance on the camera chip without having areas of over-exposure. The measured side-on radiances result from the local emission coefficients integrated along the line of sight through the arc. These can be reconstructed

in cylindrical coordinates by the inverse Abel transformation under the assumption of axial symmetry. Since the measurement of side-on radiances is simultaneously performed for two spectral intervals of the same measurement object, the coordinates of the resulting emission coefficient distributions can be superimposed and local emission ratios can be calculated for each corresponding pixels. These components are compared with calculated emission ratios within the filter widths yielding the local plasma temperature. The temperature dependency of each calculated emission coefficient for corresponding spectral interval as well as the resulting ratio are described in detail in [22].

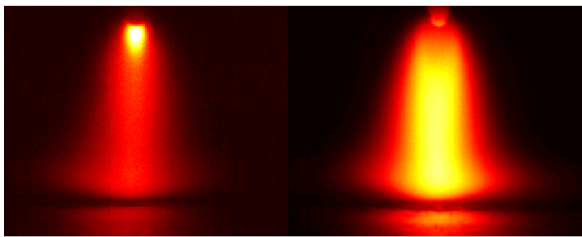


Figure 3: Plasma emission measured with setup from Figure 2 on a single camera chip. (The bottom part of the picture shows reflections from the anode.) Left: Plasma emission from 487.5 to 488.5 nm. Right: Plasma emission from 689 to 699 nm. (In order to approximate the appearance of the original 12 bit image, colour conversion and tone mapping was applied before compression to 8 bit.)

Due to the characteristics of the spectral emission temperature measurements with this approach can be performed up to 26000 K. The relatively large gradients below that temperature allow for very accurate temperature measurements in the range of 15000 K to 25000 K. At lower temperatures the accuracy of the measurement decreases since small variations in the measured ratios lead to relatively large variations in the resulting temperature. The accuracy of the measured ratios can be determined based on the camera resolution and the standard deviation of the error due to the inverse Abel transform.

An example of the camera-system-obtained temperature distribution inside the TIG arc is shown in figure 4. Due to the fact that a high speed camera is used high temporal resolution can be achieved. In order to show the capability of the camera-based setup to determine three-dimensional plasma temperature distributions with a high time-resolution the experiments subsequently performed make use of an unsteady TIG process.

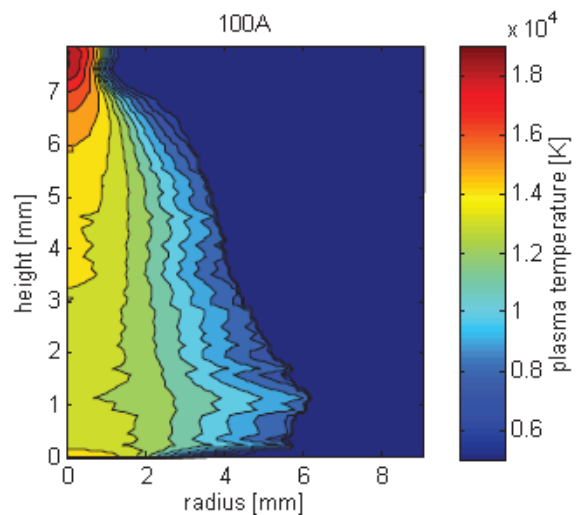


Figure 4: Resulting plasma temperatures for a current of 100A. The contour plots show the radial and axial decrease of temperature from the hot cathode region. Each surface color indicates a temperature interval of 1000 K

The TIG arc in this experiment was recorded with 33000 frames per second (fps). Figure 5 shows the temperature evolution of the arc 2 mm below the cathode on the arc axis ($r=0\text{mm}$). The corresponding current signal was measured with a calibrated Hall-effect device (Honeywell SS94A1F).

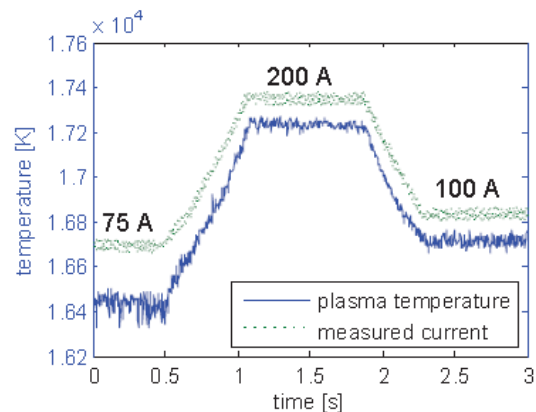


Figure 5 Plasma temperature reacting to a transient current flow in the plasma.

In addition the radial position of isotherms of plasma temperature was observed. The result is shown in figure 6.

The modulation of the arc radius is clearly visible which allows the determination of the footprint of the arc which, in the case of welding, is an important property for weld pool heating and thus weld pool geometry.

The uncertainties of the temperature determination are produced by two effects—random errors of the measurements and systematic errors due to assumptions concerning plasma radiation. Systematic errors can be

caused for example by the departure from LTE and by a non-negligible optical thickness of the observed atomic line.

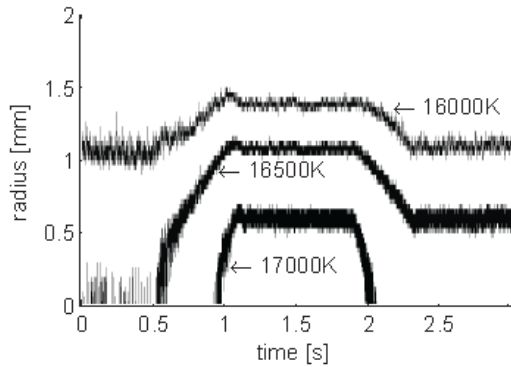


Figure 6: Radial Isotherm position reacting to current change as shown in figure 5

The effects to be analyzed become more complicated in the gas metal arc welding (GMAW) process. Pulsed currents as shown in figure 5 are increasingly used to determine the size of the droplets which stem from a wire electrode, geometrically replacing the cathode in TIG welding but here used with a positive polarity. These droplets determine weld quality and produce metal vapor which changes the plasma parameters thus the generation of the droplet and the trajectory and interaction with the plasma are important parameters for welding purposes. For characterization various attempts to measure droplet parameters have been made, two of which are introduced in this paper. The first one involves the determination of droplet temperature by using pyrometry. In GMAW the emissivity of molten metal is not known with sufficient accuracy and can vary locally due to oxidation, temperature variations and surface texture. Using two-color-pyrometry surface temperature can be determined without knowledge about the emissivity. Assuming black body radiation the emissivity coefficient is canceled out due to the use of intensity ratios. Using the assumption that the emissivity ε_1 and ε_2 at the wavelengths chosen ($\lambda_1=780$ nm and $\lambda_2=940$ nm) does not differ significantly the temperature for black body can be described by:

$$T = \frac{\frac{hc}{k_B} \left(\frac{1}{\lambda_2} - \frac{1}{\lambda_1} \right)}{\ln\left(\frac{\varepsilon_1}{\varepsilon_2}\right) + 5 \cdot \ln\left(\frac{\lambda_1}{\lambda_2}\right)} \quad (1)$$

where h is the Planck constant, c the speed of light and k_B the Boltzmann constant.

To perform the pyrometry an optical setup similar to the one shown in figure 2 is used. The object of interest is observed through an objective. The collected light is divided into two beams by a mirror prism. Both beams are projected onto a low light performance CMOS image sensor of a high speed camera (pco dimax) by two mirrors. In both beam paths an interference filter of the different wavelengths is placed, producing a single image on the sensor chip displaying two images of the same droplet (figure 7). The surface temperature of the observed object is determined by ratio generation of the intensity at both wavelengths.

The system is calibrated by a tungsten ribbon lamp.

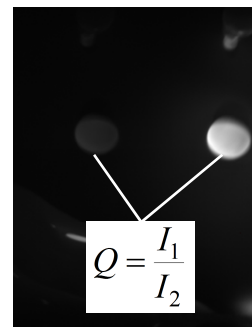


Figure 7. raw image of droplet emission at two different wavelengths

Using this setup the droplet can be observed with high temporal resolution. Two-color-pyrometer measurements show especially for low wire feed rates that the droplet is not heated uniformly by the arc. The bottom where apparently most of the arc energy is deposited during current conduction before detachment is hotter than the top part of the droplet, where a kind of pinch effect takes place. On the trajectory to the workpiece the droplet temperature equalizes with the result that the average temperature decreases, figure 8. The homogenization of surface temperature confirms the observation of [23].

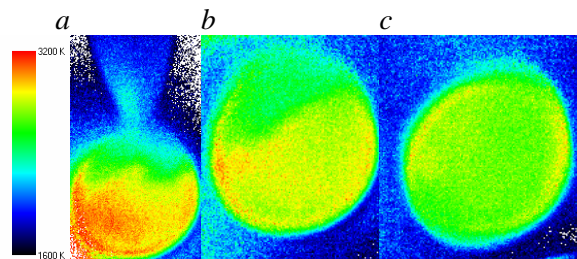


Figure 8. Temperature distribution of the droplet surface while traveling to the workpiece, before detachment (a), after detachment (b), at height of cathode (workpiece) (c)

In addition numerous fundamental studies have been carried out to determine the surface tension

and viscosity of molten metal droplets or metal pools as a function of temperature, composition and degree of oxidation [e.g. 24, 25] usually by analyzing the oscillation frequency of levitating droplets. *Assael et al.* [24] critically evaluated a large number of viscosity and density measurements and employed trustworthy results in a linear regression analysis as a function of temperature. The work clarifies the difficulties and uncertainties in determining viscosity even under very ideal conditions, such as microgravity carried out in space lab missions or parabolic flights. Here, the oscillating drop method has been used for the first time to determine surface tension and viscosity of droplets in GMAW processes [e.g. 26 and references therein]. After detachment from the wire electrode the droplet performs a significant natural oscillation about its sphere which is analyzed during the free fall to the workpiece which can be described by a symmetrical damped oscillation. The oscillation is detected using high-speed imaging similar to the systems described above with high temporal resolution.

The analysis method is based on the fact that the frequencies of the surface oscillations of a liquid droplet free from other forces are related to the surface tension σ as proposed by *Rayleigh* [27] and corrected for an earthbound oscillation by *Cummings* [28]:

$$\sigma = \frac{\pi^2 r^3 \rho}{2T^2} \quad (2)$$

where ρ is the density of the liquid, r the radius of the droplet and T the period of oscillation of the lowest frequency mode. As a result of the viscosity of the metal, the oscillation is damped. From the work of *Chandrasekhar* [29], the relationship between the decay time of the oscillation and viscosity is known. The viscosity μ is given by:

$$\mu = \frac{r^2 \rho}{5\tau} \quad (3)$$

τ is the damping constant. In order to apply this formula, the following three conditions must be met:

1. the geometry of the droplet must be spherical,
2. the oscillation must persist undisturbed for the time $t = 1/\tau$
3. no additional damping mechanism.

In turn, from the surface tension or viscosity the temperature can be derived based on the known

relationships of temperature and surface tension or viscosity. The great advantage of this contactless method is that the welding process is not influenced by the measuring technique itself. Using this method the temperature measurements using two-color pyrometry were verified.

3. THERMAL SPRAY APPLICATIONS

With simulation progressing at fast rate, the need for verification is growing, especially with respect to temperature and gas velocity distribution in the jet. While progress has been made in both areas, this paper will concentrate on new results of the temperature measurement obtained with computer tomography (CT) [30]. The principle setup is shown in figure 9.

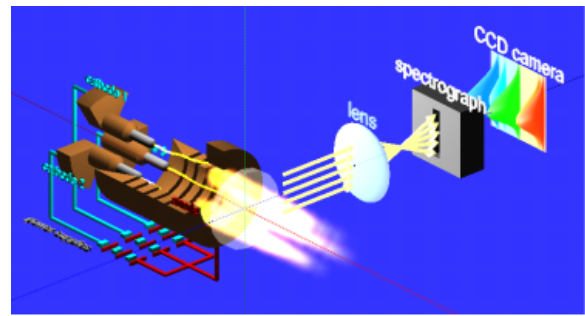


Figure 9: Experimental setup for emission computer tomography; the camera is circling the object (plasma jet)

Using CT it is possible to spectroscopically measure plasma temperatures of a non-rotationally-symmetric jet as no Abel inversion is required. For that purpose 60 individual measurements are made at 60 different angles around a half circle of the jet. Analysis of the results, however, has to rely on temporal stability of the object examined as the images are taken subsequently during a time span of a few seconds. Hence its primary application lies on the more stable thermal spray torches.

Using the setup shown in Figure 9 only a small cross section of the plasma jet can be investigated as with any regular spectrograph the 2D image obtained represents the intensity of the radiation entering the entrance slit versus the wavelength of the radiation. An investigation of the complete jet would therefore require numerous measurements along the axis of the plasma jet. In order to increase the field of view the CT system has been modified to allow for spectroscopic measurement without the use of a spectrograph.

For that purpose the CT system was modified to use 3 individual cameras (Figure 10) on a single turning unit. Each of these cameras is moved in

3°-steps 180° around the plasma jet. The images obtained cover ~35 mm along the jet axis, from which, limited by the CCD (60x60) resolution, 60 cross sections are reconstructed.

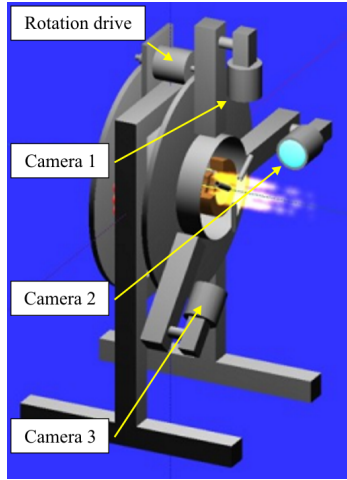


Figure 10: Experimental setup using three CCD cameras

The resolution is thus $0.25 \times 0.25 \text{ mm}^2$ per pixel. In order to be able to measure plasma temperatures the three cameras were each equipped with an interference filter of either range: 1) 689-699 nm, 2) 761-771 nm and 3) 825-835 nm. For every cross section an intensity distribution in the defined wavelength interval was reconstructed (Figure 11).

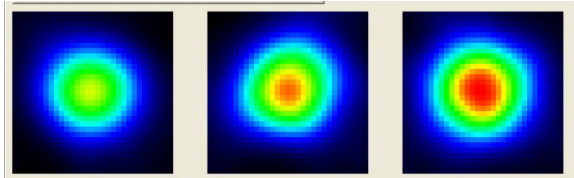


Figure 11: DeltaGun: tomographically reconstructed cross sections of emissivity for an Argon plasma jet (gas flow 30 slpm Argon, current 340 A, power 36 kW) for three different wavelength intervals

Using the measured ratios of intensity for each position and two wavelengths at a time and comparing these ratios to the computed values for radiation emitted at LTE conditions the temperature at this point can be determined similar to the spectroscopic measurements described for welding. The procedure is described in detail in [21].

. In order to test this setup a DeltaGun by GTV was used at fairly low power settings (current 340 A, power 36 kW). Figure 12 shows the results of this measurement for a cross section ~1cm downstream of the nozzle exit. A maximum temperature close to 14000 K was measured and interestingly enough no triangular structure could be observed. It might be that a the

considered relative low power level, the cold and thus massive Argon flow injected laterally at the anodes is enough to “delete” the footprint of the hot three short anodic arcs.

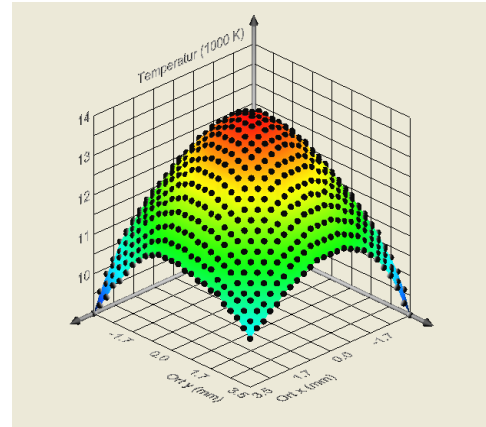


Figure 12: Temperature profile of DeltaGun for a cross section close to nozzle (gas flow 30 slpm Argon, current 340 A, power 36 kW)

This observed temperature at the plasma jet axis is compatible with a simple estimation of the radial velocity (4) and temperature profile (5) at the torch outlet. Due to the axial symmetry of the flow within the DeltaGun for most of its length, the velocity and temperature at the nozzle are assumed in a first approximation as having cylindrical symmetry

$$v_{axial}(r) = v_{max} \left[1 - \left(\frac{r}{R} \right)^m \right] \quad (4)$$

$$T(r) = T_{max} \left[1 - \left(\frac{r}{R} \right)^n \right] + T_{wall} \quad (5)$$

which, according to the CT measurements just discussed, is still maintained even after the anode ring. In the previous equation R denotes the nozzle radius, T_{wall} is the anode wall temperature (taken here as 300 K) and exponents $m=2$ and $n=4$ have been assumed, similar to those of a laminar stationary flow within a cylinder. Although the flow close to the outlet is certainly not laminar, and therefore a rather flat radial profile for velocity/temperature (large exponents m and n) can be expected. Due to an injection of an additional Argon shroud at the anode segments a cold layer at the plasma core fringes occurs near to the nozzle, leading to a more pronounced radial profile for velocity and temperature. Using the equilibrium thermodynamical plasma gas properties for Argon (density ρ and enthalpy density h) listed in [16], the central velocity v_{axial} and temperature T_{max} at the nozzle can be estimated to match the

effective power P_{eff} (6) as well as the gas mass flow dm/dt (7) injected into the plasma torch

$$P_{eff} = \int_0^R \rho(T(r))v_{axial}(r)h(T(r))2\pi r dr \quad (6)$$

$$dm/dt \approx \int_0^R \rho(T(r))v_{axial}(r)2\pi r dr \quad (7)$$

For the case considered, with a nozzle radius $R=3.5\text{mm}$, a mass flow of $dm/dt=30+20\text{smlm Ar}$ (the additional 20 slm Ar injected at the three anodes in order to protect them) and an effective power of $P_{eff}=0.5 \times 36\text{kW}$ (50% measured thermal efficiency), the resulting maximal temperature at the plasma jet axis reaches 13700 K (combined with a central velocity of 1850 m/s), close to the experimental result obtained by means of CT.

In addition the emissivity profile of a gas jet produced by an HVOF torch is measured by means of a computer tomography system for least two different wavelengths. Based on the two color pyrometry approach the 3D temperature profile of the torch is reconstructed using the measured emissivity data. Assuming an optically thin gas jet, the temperature distribution inside such a jet can be determined by measuring the intensity emitted by soot particle inside the jets along different angles, followed by a tomographic reconstruction of the local emissivity at each location inside the gas as described in [30].

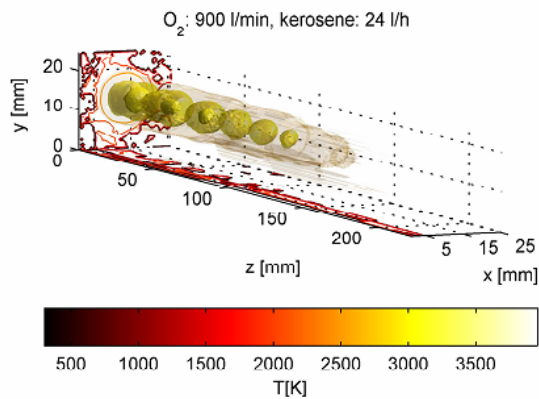


Figure 13: Tomographic reconstruction of temperature distribution; GTV K2 gun operating with 24l/h kerosene and 900l/min O₂

The tomographic measurements were performed on a GTV K2 HVOF gun operating with 24l/h kerosene and 900l/min O₂. The emissivity distribution for two narrow spectral windows at $694 \pm 5\text{nm}$ and at $766 \pm 5\text{nm}$ was measured for the complete HVOF flame reconstructed from 6 separate tomographic scans in downstream

direction from the torch outlet. The scans have an overlap of 5mm, which allows reconstructing the shape of a 200mm long flame. The torch outlet is located at $z = 0\text{mm}$ and the gas jet is flowing downstream along the axial coordinate z .

The resulting temperature distribution calculated using the obtained emissivity profiles is shown in figure 13, with a maximum gas temperature of approximately 2300K at the torch outlet. The reconstruction yields a higher temperature (above 3000K) inside the Mach diamonds. However, the temperature inside the compression region may not be correct since in that region the flame may no longer be assumed to be optically thin.

4 RESULTS AND DISCUSSION

Four innovative optical diagnostic systems have been introduced. A high-speed spectroscopic system for transient plasmas, a fast two color pyrometer for droplet analysis in welding applications, an imaging technique to evaluate droplet oscillations and a computer tomography system applying the spectroscopic and pyrometric techniques to non-rotationally symmetric thermal plasma systems. The systems are based on the use high-speed imaging to obtain temporal resolution and can be applied to numerous thermal and non-thermal plasma processes wherever spectroscopic analysis of transient processes is required. The systems require careful calibration but are subsequently fairly robust and easy to use when fundamental spectroscopic analysis knowledge is available.

The key to successful use is the application of the innovative imaging system that allows acquiring two (or more) images on one single chip thereby providing perfect temporal synchronicity. With improving camera technology (larger CCD chips, higher frame rate) the possibilities of these systems will increase and provide further opportunities for obtaining more detailed information.

REFERENCES

- [1] Bosworth M R and Deam R T "Influence of GMAW droplet size on fume formation rate" J. Phys. D: Appl. Phys. **33** 2605–10 (2000)
- [2] Deam R T, Simpson S W and Haidar J "A semi-empirical model of the fume formation from gas metal arc welding" J. Phys. D: Appl. Phys. **33** 1393-1402 (2000)
- [3] Jenkins N T, Mendez P F and Eagar T W "Effect of arc welding electrode temperature

- on vapor and fume composition" Trends in Welding Research, Proceedings of the 7th International Conference (2005)
- [4] Murphy A B "The effects of metal vapour in arc welding" *J. Phys. D: Appl. Phys.* **43** 434001 (2010)
- [5] Tanaka M and Lowke J H "Predictions of weld pool profiles using plasma physics." *J. Phys. D: Appl. Phys.* **40** R1–R23 (2007)
- [6] Fan H G and Kovacevic R "Dynamic analysis of globular metal transfer in gas metal arc welding - a comparison of numerical and experimental results" *J. Phys. D: Appl. Phys.* **31** 2929-41 (1998)
- [7] Haidar J "A theoretical model for gas metal arc welding and gas tungsten arc welding. I." *J. Appl. Phys.* **84** 3518-29 (1998)
- [8] Haidar J "An analysis of heat transfer and fume production in gas metal arc welding. III." *J. Appl. Phys.* **85** 3448-59 (1999)
- [9] Schnick M., Wilhelm G., Lohse M., Füssel U., Murphy A.B "Three-dimensional modelling of arc behaviour and gas shield quality in tandem gas-metal arc welding using anti-phase pulse." *J. Phys. D Appl. Phys.* **44** 185205 (2011)
- [10] Moradian A and Mostaghimi J "Surface tension measurement at high temperatures by using dynamics of melt flow." *J. of Fluid Eng.* **129** 991-1001 (2007)
- [11] Nemchinsky V A "Heat transfer in a liquid droplet hanging at the tip of an electrode during arc welding" *J. Phys. D: Appl. Phys.* **30** 1120–1124 (1997)
- [12] Siewert E., J. Schein and G. Forster "Determination of enthalpy, temperature, surface tension and geometry of the material transfer in PGMAW for the system argon–iron." *J. Phys. D: Appl. Phys.* **46**(22) 224008 (2013)
- [13] D. Hawley, A. Refke, K. Landes, "Plasma plume condition forming of cascaded type plasma guns", *Proc. Int. Thermal Spray Conf. Basel* (2005)
- [14] P. Fauchais, G. Montavon, M. Vardelle, J. Cedelle, "Developments in direct current plasma spraying", *Surf. Coat. Technol.*, **201**(5), 1908-1921 (2006)
- [15] L. Pawlowski, "The Science and Engineering of Thermal Spray Coatings", John Wiley & Sons, Hoboken, (2007)
- [16] M. Boulos, P. Fauchais, E. Pfender, "Thermal Plasmas", Plenum Press, New York (1994)
- [17] R.N. Szente, R.J. Munz, M.G. Drouet, "Electrode erosion in plasma torches", *Plas. Chem. and Plas. Proc.* **12**(3), 327-343 (1992)
- [18] C. Chazelas, J.-F. Coudert, P. Fauchais, "Arc root behavior in plasma spray torch", *IEEE Trans. on Plas. Sc.*, **33**(2), 416-417 (2005)
- [19] Z. Duan, J. Heberlein, "Arc instabilities in a plasma spray torch", *J. Therm. Sp. Tech.*, **11**(1), 44-51 (2002)
- [20] J. Schein, J. Zierhut, M. Dzulko, G. Forster, K. Landes, "Improved Plasma Spray Torch Stability Through Multi-Electrode Design", *Contr. Plas. Phys.* **47**(7), 498-504 (2007)
- [21] J.-L. Marques, G. Forster, J. Schein, "Multi-Electrode Plasma Torches: Motivation for Development and Current State-of-the-Art" *The Open Plasma Physics Journal*, **2**(10), 89-98 (2009)
- [22] B Bachmann et al "High-speed three-dimensional plasma temperature determination of axially symmetric free-burning arcs" *J. Phys. D: Appl. Phys.* **46** 12520 (2013)
- [23] Yamazaki, K., Yamamoto, E., et al. "The measurement of metal droplet temperature in GMA welding by infrared two-colour pyrometry" *Weld. Intern.* **24**(2), 81–87 (2010)
- [24] Assael M J, Kakosimos K, Banish R M, et al "Reference Data for the Density and Viscosity of Liquid Aluminum and Liquid Iron" *J. Phys. Chem. Ref Data*, **35**, 285-300 (2006)
- [25] Moradian, A., Mostaghimi, J. "High Temperature Surface Tension Measurement." *IEEE Trans. on Plas. Sc.*, **33**(2) (2005)
- [26] Bachmann B, Siewert E and Schein J "In situ droplet surface tension and viscosity measurements in gas metal arc welding" *J. Phys. D: Appl. Phys.*, **45**, 1-10 (2012)
- [27] Rayleigh L "On the capillary phenomena of jets" *Proc. R. Soc. Lond.* **29** 71–97 (1879)
- [28] Cummings, D.L. and Blackburn, D.A. "Oscillations of magnetically levitated aspherical droplets" *J. Fluid. Mech.* **224**, 395–416 (1991)
- [29] Chandrasekhar S "Hydrodynamic and hydro magnetic stability" University of Chicago, Dover Publications, Inc. New York 466-7 (1981)
- [30] J. Schein, M. Richter, K. Landes, G. Forster, J. Zierhut, M. Dzulko, "Tomographic Investigation of Plasma Jets Produced by Multielectrode Plasma Torches", *J. Therm. Spray Technol.* **17**(3), 338-343 (2008).